Heterodyne-Detected Fifth-Order Nonresonant Raman Scattering from Room Temperature CS_2

Laura J. Kaufman, Jiyoung Heo, Larry D. Ziegler,* and Graham R. Fleming

Department of Chemistry, University of California, Berkeley, California 94720 and
Physical Biosciences Division, Lawrence Berkeley National Laboratory, Berkeley, California 94720

(Received 26 October 2001; published 30 April 2002)

Actively phase-locked heterodyne-detected fifth-order nonresonant Raman scattering from room temperature CS_2 has been measured. The experimental signals have similar magnitudes, shapes, and sign changes as calculated responses obtained via molecular dynamics simulations [S. Saito and I. Ohmine, Phys. Rev. Lett. **88**, 207401 (2002)]. The measured signals contain sign changes that appear to be associated with the coupling of rotational motions both to each other and to translational motions.

DOI: 10.1103/PhysRevLett.88.207402 PACS numbers: 78.30.Cp, 61.20.Lc

One of the major unsolved questions in ultrafast liquid dynamics is how diffusive dynamics (i.e., those involving structural change) emerge from the fluctuations of individual molecules around their equilibrium positions. This question is intimately related to that of energy flow between different degrees of freedom in the liquid and ultimately to the flow of energy between solutes and solvents which initiate chemical reactions and stabilize products once barriers are crossed. The challenge of developing a spectroscopic technique that can probe the intermolecular frequencies characteristic of liquid motions, and their couplings with each other, has proved technically demanding. The need for a nonresonant form of photon echo spectroscopy, capable of eliminating the ensemble average broadening inherent in linear spectroscopy, was recognized by Tanimura and Mukamel, who proposed a fifth-order Raman measurement, initially as a probe of spatial heterogeneity [1,2]. In the experiment, two pump pulses prepare a vibrational coherence. After a time t_1, a second set of pulses transfers this vibrational coherence to a second vibrational coherence. After a time t_2, the second coherence is probed. It was quickly realized that this measurement also probes couplings between different nuclear motions and thus possesses the potential to provide qualitatively new insights into the anharmonic dynamics of liquid motion. The technique has, in principle, wide applicability to condensed phase dynamical problems, such as the question of spatial heterogeneity of liquids near the glass transition, or determination of biopolymer structure (with femtosecond time resolution) through space coupling of specific vibrational modes. The full potential of nonlinear optical spectroscopy is realized only when the full signal field, rather than the signal intensity, is measured, since only then can sign changes be determined and linear combinations of different signals be created to characterize the response [3]. In this Letter, we report actively phase-locked heterodyne detection of the fifth-order Raman signal from liquid CS_2. We believe that this is the first measurement to obtain the fully nonresonant $R^{(5)}$ response, avoiding complications from the presence of either $R^{(3)}$ and absorptive portions of third-order cascade signals in the intrinsic heterodyne experiment [4] or two-photon absorption in the two-color experiment [5]. Earlier homodyne measurements for CS_2 were severely compromised by the presence of cascade signals, which emerge in an experimentally undifferentiable direction from the fifth-order signal [6]. These signals are generated when a third-order process occurs on one oscillator and the emitted field from that event acts as either a pump or probe field for a second third-order event on another oscillator. Two methods are used to minimize cascade contributions to our signals: (i) phase mismatching the first step of each cascade [7] and (ii) using heterodyne detection to eliminate cross terms between residual cascades and the fifth-order signal. The new heterodyne data show remarkable and unanticipated changes in signal sign in the two-dimensional response, which are very similar to the sign changes observed in Saito and Ohmine's simulation of the same system [8]. These nodal lines are signatures of electrical anharmonicity [or nonlinear polarizability (NL)] and/or mechanical anharmonicity (MA); thus, they are signatures of coupling between different degrees of freedom in the liquid.

Briefly, 1 nJ, 28 fs (Gaussian, FWHM) pulses centered at 800 nm are generated in a standard Ti:sapphire oscillator. The pulses are regeneratively amplified, resulting in 30 μJ, $\sim$60 fs pulses at 1.5 kHz. The output is split into six beams (the sixth beam acts as a tracer to assist in the alignment of the signal) of nearly equal intensity that are focused into a 1.0-mm-long static sample of CS_2 by a 5.08 cm diameter, 28.9 cm focal length singlet quartz lens [7]. The beam size at the sample is $\sim$150 μm. The polarization of each beam is individually adjustable by a $\lambda/2$ plate. Power is adjusted to $\sim$3 μJ/pulse at the sample. Mechanical stages provide the t_1 and t_2 time delays.

Homodyne-detected fifth-order signals are collected to ensure consistency with previously collected results. Then, the signal and beam 5, employed as both probe and local oscillator (LO), are directed into an interferometer, where they are overlapped spatially and temporally (Fig. 1). To maintain the relative phase of the local oscillator and the signal, active phase locking, which has been shown effective for third-order nonresonant spectroscopies [9], is

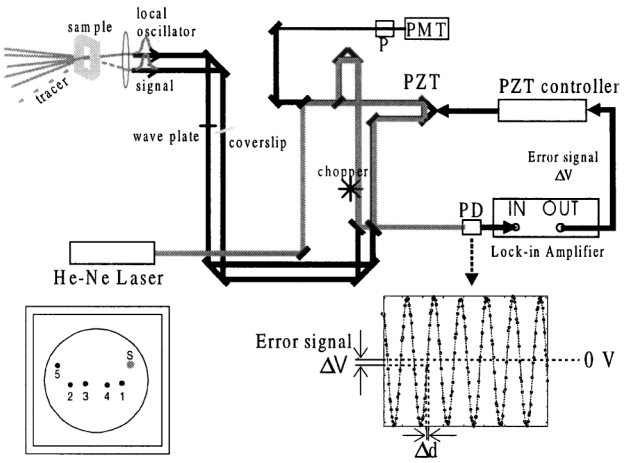

FIG. 1. Actively phase-locked heterodyne interferometer. The paths of the signal and local oscillator are black. The coverslip is used to set the relative phase of the signal and LO. The He-Ne laser beams are depicted in gray. PZT is the piezoelectric transducer, P is an analyzer polarizer, PMT is a photomultiplier tube, and PD is a photodiode. The graph shows a He-Ne interference pattern as monitored while sweeping one arm of the interferometer. Change in voltage detected on the PD acts as an error signal to maintain path lengths to within $\pm 6°$ over the ~ 1 hour necessary to collect a fifth-order surface. The inset shows the geometry of the incoming beams (and signal) at the focusing lens.

used. The phase stability is similar to that obtained via diffractive optic techniques [10]. Active phase locking is achieved by detecting an error signal (change in voltage) from He-Ne laser beams that traverse the same paths as the signal and LO. The error signal is fed to a piezoelectric transducer (12 nm resolution) that adjusts one arm of the interferometer to counteract any change in path length that has occurred. Phase stabilization is also necessary between pulses 1 and 2 and between pulses 3 and 4; however, this can be simply achieved by enclosing the entire experimental apparatus in boxes. The phase of the LO relative to the signal is set by maximizing total amplitude at $t_1 = t_2 = 120$ fs by rotating the angle of the coverslip in the signal line [10]. If only one (fully nonresonant) signal is being measured, this ensures measurement of the desired signal. However, because of the possibility of the presence of cascades, 180° phase shifted from the fifth-order signal in this geometry, such a procedure only ensures maximizing the dominant signal at this point. A point close to the axis is chosen to reduce the likelihood of cascade contamination (which, because of different frequency weightings [11], is more likely at long times). In the heterodyne detection scheme the signal is chopped, necessitating the removal of homodyne contributions.

Several tensor elements of the fifth-order signal have been collected via heterodyne detection, including R_{zzzzzz}, R_{zzyyzz}, R_{zzyyyy}, R_{zzmmzz}, R_{zzllzz}, and R_{zzzzmm}. Polarizations read from right to left, "m" is the magic angle (54.7°) chosen so as to provide discrimination against cascades, and "l" is an angle (60°) that suppresses cascade contributions even more fully [12]. Figure 2 shows the R_{zzmmzz} and R_{zzzzmm} surfaces. The R_{zzzzmm} surface (and slices) have not had homodyne portions removed because the homodyne signal was at the noise level. The LO:signal intensity ratio was 40:1. The homodyne contribution has been removed from the R_{zzmmzz} signal (and slices). The R_{zzzzmm} surface is smaller in amplitude than other measured tensor elements. It has a large signal in the region of the $t_2 = 0$ axis, as well as a signal in the region of $t_1 = 0$. In the region of that axis, the signal contains a node. A slice taken on the $t_1 = 0$ axis is mostly negative and peaks at ~ 250 fs (we estimate error to be ± 10 fs in all cases), while a slice taken at $t_1 = 100$ fs is positive and peaks at ~ 150 fs. The signal in the two-dimensional part

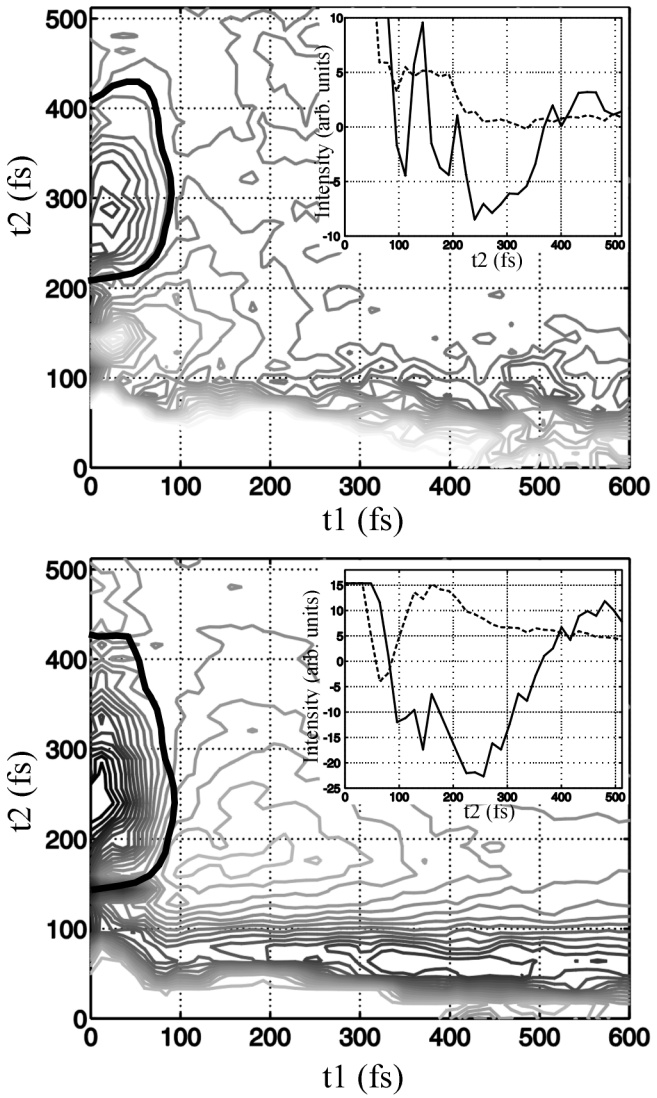

FIG. 2. (top) Measured R_{zzzzmm} surface (25 contours). Inset shows $t_1 = 0$ (solid line) and $t_1 = 100$ fs (dashed line) slices from the surface. (bottom) Measured R_{zzmmzz} surface. Inset shows $t_1 = 0$ (solid line) and $t_1 = 100$ fs (dashed line) slices from the R_{zzmmzz} surfaces. The measured surfaces have solid lines indicating the approximate position of the nodal planes.

of the spectrum ($t_1, t_2 > 0$) extends to ~220 fs in both dimensions. The R_{zzmmzz} signal has a longer extension into the two-dimensional area, with signal persisting to >400 fs in both dimensions. This surface also has significant amplitude around both axes and again displays a change in sign. A slice taken at $t_1 = 0$ is negative and peaks at ~250 fs, while one taken at $t_1 = 100$ fs is positive and peaks at ~175 fs. These characteristics are in remarkable agreement with those seen in the molecular dynamics (MD) simulations [8].

While finite field MD calculations suggest that even the magic angle signals collected in our phase-matching geometry will not provide adequate discrimination against cascades [13], the striking agreement between our magic angle signals and the MD simulations suggests that the size of $R^{(\mathrm{cas})}/R^{(5)}$ calculated by Jansen *et al.* [12] is an overestimate. Their calculations show that for our phase-matching geometry in the case of R_{zzmmzz}, for example, the largest cascade contributor will be ~1.4 times larger than the fifth-order signal. This estimate is made using the largest values of the third- and fifth-order responses; however, because those maxima occur at different locations in the two signals, it is possible that while some portions of the signal are dominated by cascades (most likely long time portions) others are dominated by a fifth-order signal.

One of the striking features of the measured surfaces is the change of sign from negative to positive in the region of the $t_1 < 0$ fs axis (insets of Fig. 2). This change is also evident in the MD simulations [8]. The slice of the measured signal along $t_1 = 0$ contains both a hyperpolarizability (or electronic fifth-order signal) $\langle[\alpha(t_2), \gamma(0)]\rangle$ (not included in MD simulations) and nuclear fifth-order signal $\langle[\alpha(t_1 + t_2), \alpha(t_1)], \alpha(0)\rangle$. The nuclear signal present on $t_1 = 0$ is unique in that it probes population dynamics [13]. Also, any residual cascade contributions from either the front ($t_1 > 0$ fs) or back quadrant ($t_1 < 0$ fs) will exist here if contamination is present, though cascade simulations (constructed from measured third-order data and knowledge of geometry-determined phase-matching factors) are generally unable to reproduce the signal for $t_1, t_2 < 400$ fs (especially for signals with m and l components). Examination of the relative amplitudes of the measured and simulated signals shows that the measured signal has greater (negative) amplitude than predicted in the region of the $t_1 = 0$ axis [14]. The additional amplitude may be due to the $\langle[\alpha(t_2), \gamma(0)]\rangle$ hyperpolarizability. The similarity in the locations of the nodes in the measured and simulated fifth-order signal suggests that the hyperpolarizabilities are of the same sign as the nuclear fifth-order signal in that region. The presence of a hyperpolarizability component along the $t_1 = 0$ axis is not surprising since the measured signals show $\langle[\gamma(t_1), \alpha(0)]\rangle$ hyperpolarizability signals (or cascade contamination) along the $t_2 = 0$ axis, where no nuclear fifth-order signal can exist [2]. The signal around this axis (which has both positive and negative regions in most tensor elements) appears larger than that around $t_1 = 0$. This is not unexpected: $\langle[\gamma_{zzzz}(t_1)\alpha_{mm}(0)]\rangle$ and $\langle[\gamma_{zzmm}(t_1), \alpha_{zz}(0)]\rangle$ signals are not necessarily of the same magnitude as $\langle[\alpha_{zz}(t_2), \gamma_{zzmm}(0)]\rangle$ and, in the expression for the fifth-order signal, there is an additional factor of $1/2$ in front of the $\langle[\alpha(t_2), \gamma(0)]\rangle$ hyperpolarizablity [15].

The sign change evident in the nuclear portion of most tensor elements of the fifth-order signal is unique in that, to our knowledge, no such sign changes have been seen in third-order nuclear birefringent responses of liquids. As pointed out in the adjoining paper, the sign change is related to the detailed rotational and translational dynamics in the liquid [8]. Instantaneous normal mode studies of the third-order polarizability weighted densities of states (PWDOS), frequency dependent quantities proportional to signal amplitude, show that cross terms between collision-induced (CI) and librational portions of the PWDOS are often negative with respect to the individual terms, though the overall PWDOS are always of one sign [11]. Interestingly, the cross terms between librational and CI terms are generally of the same sign in the fifth-order PWDOS, though these calculations were based on NL only and did not include $n \neq m$ mode-mode couplings [16]. Detailed MD studies of the two, three, and four body terms that may contribute to the third-order signal show that isotropic-anisotropic cross terms can lead to contributions to the response function that change sign in time [17]. Similar calculations for the fifth-order signal would be valuable in determining the origin of the positive and negative portions of the signal, especially since it has been shown that first shell interactions are the most important ones in the fifth-order signal [8,18]. Such analysis, coupled with polarization analysis [19], can reveal why certain tensor elements (such as R_{zzyyyy}) lack a node and the detailed dynamics that give rise to this node in other tensor elements.

Another interesting feature of the measured surfaces is the time scale of the decay of the diagonal slices, where the experimental results and MD simulations show some agreement (Fig. 3). In terms of relative magnitudes of the signal, the agreement is very good. Figure 3 presents the sizes of the measured signals relative to each other without any normalization of individual slices with respect to the matching MD signals. (Homodyne portions have not been removed, but have no effect on the peak position or relative amplitude of the slices. The sign of the R_{zzyyyy} signal was chosen to be in accord with the MD simulation, since relative signs between tensor elements are not discernible in our experiment as performed.) The agreement in peak position and decay rate is less satisfactory. The peak positions of the measured R_{zzmmzz} and R_{zzllzz} surface occur later in time than do those in the MD simulations of these signals. The measured diagonal slices generally contain large $t_1 = 0$, $t_2 = 0$ and $\langle\zeta_{nmlkji}\rangle$ components and these may influence the nuclear peak position of the signal. The fact that the slices with hyperpolarizability components that decay the fastest have peaks closer

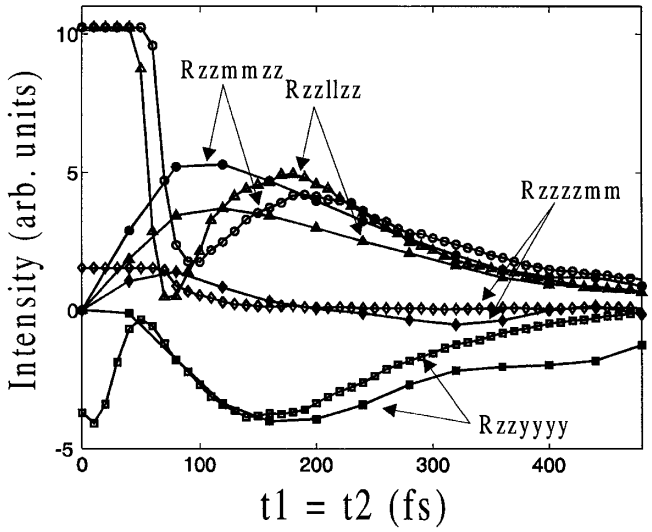

FIG. 3. Diagonal slices of several measured and simulated fifth-order signals. The lines with filled symbols are MD simulation results [14] and the corresponding lines with unfilled symbols are measured signals.

to $t_1 = t_2 \sim 100-150$ fs (thus in closer accord with MD simulations) does suggest that the hyperpolarizabilty components affect the nuclear peak position. For example, the measured R_{zzyyyy} surface has a small hyperpolarizability and a nuclear peak position at approximately $t_1 = t_2 = 150$ fs, whereas the R_{zzllzz} and R_{zzmmzz} signals have large hyperpolarizability components that dominate until $\sim$75 and 100 fs and peak positions at $\sim$175 and $\sim$200 fs, respectively.

The diagonal slice of the R_{zzmmzz} (and similar R_{zzllzz}) signal displays a slower decay than that of other tensor elements. The decay of this diagonal slice determines the time scale on which a liquid can be said to be inhomogeneous, or have memory of the original modes excited. In addition, the shape and time scale of decay of the diagonal slice may shed light on the origins of the two-dimensional Raman signal. While a quantitative decomposition into the two origins, coupling via NL and MA, is not yet available, the constant temperature velocity reassignment echo result of Ref. [8] shows that dynamical anharmonicity is an important contributor to the (diagonal slice of the) fifth-order response of CS_2 as is also the case in liquid xenon [8,20,21]. Preliminary analysis of the data reported here suggests that the shape of the signal and, in particular, the nodal structure near the $t_1 = 0$ axis arise from rotational-rotational and rotational-translational mode coupling [8], and further analysis of the nodal line structures should help pinpoint the nature of liquid motions that lead to structural change and energy flow.

We thank S. Saito, I. Ohmine, R. M. Stratt, D. R. Reichman, D. A. Blank, A. Tokmakoff, and R. J. D. Miller for stimulating discussions. We also thank S. Saito and I. Ohmine for sharing their data before publication, thus providing stimulus for this paper. This work was supported by a grant from NSF.

*Permanent address: Department of Chemistry and The Photonics Center, Boston University, Boston, Massachusetts 02215.

[1] Y. Tanimura and S. Mukamel, J. Chem. Phys. **99**, 9496 (1993).
[2] S. Mukamel, A. Piryatinski, and V. Chernyak, Acc. Chem. Res. **32**, 145 (1999).
[3] C. Scheurer and S. Mukamel, J. Chem. Phys. **115**, 4989 (2001).
[4] O. Golonzka *et al.,* J. Chem. Phys. **113**, 9893 (2000).
[5] V. Astinov *et al.,* Chem. Phys. Lett. **327**, 334 (2000); K. J. Kubarych *et al.,* J. Chem. Phys. **116**, 2016 (2002).
[6] D. A. Blank, L. J. Kaufman, and G. R. Fleming, J. Chem. Phys. **111**, 3105 (1999).
[7] D. A. Blank, L. J. Kaufman, and G. R. Fleming, J. Chem. Phys. **113**, 771 (2000).
[8] S. Saito and I. Ohmine, preceding Letter, Phys. Rev. Lett. **88**, 207401 (2002).
[9] S. Matsuo and T. Tahara, Chem. Phys. Lett. **264**, 636 (1997).
[10] M. Khalil *et al.,* J. Phys. Chem. A **104**, 5711 (2000); Q.-H. Xu, Y.-Z. Ma, and G. R. Fleming, Chem. Phys. Lett. **338**, 254 (2001); G. D. Goodno and R. J. D. Miller, J. Phys. Chem. A **103**, 10 619 (1999); L. J. Kaufman, J. Heo, L. D. Ziegler, and G. R. Fleming (unpublished).
[11] R. L. Murry, J. T. Fourkas, and T. Keyes, J. Chem. Phys. **109**, 2814 (1998).
[12] T. I. C. Jansen, J. G. Snjiders, and K. Duppen, J. Chem. Phys. **114**, 10 910 (2001).
[13] L. J. Kaufman, D. A. Blank, and G. R. Fleming, J. Chem. Phys. **114**, 2312 (2001).
[14] S. Saito and I. Ohmine (private communication).
[15] T. Steffen, J. T. Fourkas, and K. Duppen, J. Chem. Phys. **105**, 7364 (1996).
[16] R. L. Murry and J. T. Fourkas, J. Chem. Phys. **107**, 9726 (1997); R. L. Murry, J. T. Fourkas, and T. Keyes, *ibid.* **109**, 7913 (1998).
[17] H. Stassen and W. A. Steele, J. Chem. Phys. **103**, 4408 (1995).
[18] R. A. Denny and D. R. Reichman, Phys. Rev. E **63**, 065101 (2001); R. A. Denny and D. R. Reichman, J. Chem. Phys. **116**, 1987 (2002).
[19] A. Tokmakoff, J. Chem. Phys. **105**, 13 (1996); J. Cao, S. Yang, and J. Wu, J. Chem. Phys. **116**, 3760 (2002).
[20] A. Ma and R. M. Stratt, J. Chem. Phys. **116**, 4972 (2002); S. Saito and I. Ohmine, J. Chem. Phys. **108**, 240 (1998).
[21] A. Ma and R. Stratt, Phys. Rev. Lett. **85**, 1004 (2000).